

System Identification of an Aircraft Model While Considering Control Surface Actuators

Atsushi Fujimori, Katsuma Mochizuki, Shinsuke Oh-hara

Department of Mechanical Engineering, University of Yamanashi, Kofu, Yamanashi, Japan

Email: afujimori@yamanashi.ac.jp

How to cite this paper: Fujimori, A., Mochizuki, K. and Oh-hara, S. (2024) System Identification of an Aircraft Model While Considering Control Surface Actuators. *Advances in Aerospace Science and Technology*, 9, 178-190.

<https://doi.org/10.4236/aast.2024.94014>

Received: October 1, 2024

Accepted: December 23, 2024

Published: December 26, 2024

Copyright © 2024 by author(s) and Scientific Research Publishing Inc. This work is licensed under the Creative Commons Attribution International License (CC BY 4.0).

<http://creativecommons.org/licenses/by/4.0/>



Open Access

Abstract

This paper presents an identification of a continuous-time linear aircraft model while considering control surface actuators using the maximal length sequence signal. In the identification with the actuator, the input for identification is given by the command to the actuator or the output from the actuator. In the numerical simulation of longitudinal aircraft model identification, the identification performance is improved when the bandwidth ratio for the short-period mode and the bandwidth ratio between the actuator and the short-period mode are increased. Furthermore, a few input noises bring about an improvement in the identification performance. This may be effective in the case that the performance of the actuator is not sufficiently good in practical system identification.

Keywords

Aircraft Models, Actuator, Maximum-Length Sequence, Bandwidth, Subspace Identification

1. Introduction

System identification [1]-[4] is one of the most powerful techniques for obtaining a model that is needed to design control systems in several engineering fields [5]-[7]. Aircraft models needed for constructing flight control systems include several elements that are related to not only the structure of the aircraft but also aerodynamics. The modeling using system identification is, therefore, effective in obtaining the aircraft model because it avoids complicated processes such as calibration of the aerodynamic derivatives in the wind tunnel tests [8].

The authors have studied system identification for continuous-time linear aircraft models using subspace identification [9]-[12]. Subspace identification estimates the state-space matrices of the system based on the realization theory and is one of the most powerful system identification approaches for multi-input and

multi-output (MIMO) systems [3] [4]. In the previous study [11], the maximal length sequence (M-sequence) [13]-[15] was used as the identification input, and two design indexes which were related to the dynamical modes of aircraft were proposed. The effectiveness of the design indexes was demonstrated in numerical simulations. However, actuators for activating the control surfaces were not taken into consideration in the aircraft model identification [11]. It is very important from a practical point of view to understand the influence that the intermediation of the actuator has on the identification result of the aircraft model.

This paper presents a system identification of aircraft models while considering actuators for control surfaces. It may be imagined that the identification performance has deteriorated in the system identification with the actuator. In this paper, the deterioration factors are investigated from the viewpoint of the frequency characteristics. A technique for suppressing the deterioration is also discussed through identification calculation.

The rest of this paper is organized as follows. Section 2 briefly presents the aircraft model in longitudinal motion, which is to be identified in this paper. Section 3 presents the procedures of the subspace method for identifying the continuous-time linear system. The choices of input and output for identification are presented for the system identification with the actuator. Section 4 presents the setup for identification: M-sequence, which is used as the command signal to the actuators, identification indexes and evaluation methods of identification results. Numerical simulation is presented in Section 5. Concluding remarks are given in Section 6.

2. Linear Aircraft Model

A model to be identified in this paper is a linear aircraft model in longitudinal motion. This section briefly presents a state-space equation with aerodynamic derivatives. The longitudinal motion of an aircraft is described using the following state-space equation [8].

$$\begin{cases} \dot{\mathbf{x}}_{lon}(t) = \mathbf{A}_{lon}\mathbf{x}_{lon}(t) + \mathbf{B}_{lon}\mathbf{u}_{lon}(t) \\ \mathbf{y}_{lon}(t) = \mathbf{C}_{lon}\mathbf{x}_{lon}(t) \end{cases} \quad (1)$$

where the state, input and output vectors, denoted as \mathbf{x}_{lon} , \mathbf{u}_{lon} and \mathbf{y}_{lon} , are

$$\mathbf{x}_{lon} \triangleq [u \quad \alpha \quad q \quad \theta]^T, \quad \mathbf{u}_{lon} \triangleq [\delta_e \quad \delta_t]^T, \quad \mathbf{y}_{lon} \triangleq [u \quad q]^T. \quad (2)$$

The elements of \mathbf{y}_{lon} are selected as a suitable variable for identification [12]. The characteristic equation of the longitudinal dynamical modes is written as

$$|s\mathbf{I} - \mathbf{A}_{lon}| = (s^2 + 2\zeta_{sp}\omega_{sp}s + \omega_{sp}^2)(s^2 + 2\zeta_{lp}\omega_{lp}s + \omega_{lp}^2) = 0, \quad (3)$$

where ζ_{sp} and ω_{sp} are the damping factor and the natural frequency of the short-period mode, while ζ_{lp} and ω_{lp} are those of the long-period mode. Generally, we have the following relations: $0 < \omega_{lp} < \omega_{sp}$ and $0 < \zeta_{lp}, \zeta_{sp} < 1$ [8].

3. System Identification Using Subspace Identification Method

This section describes procedures for identifying the continuous-time linear time-

invariant (LTI) system using subspace identification. Since the subspace identification method estimates a model as the discrete-time system, the estimated model is inversely transformed into a continuous-time model. System identification with the actuator is described in the next.

3.1. Identification of Continuous-Time LTI System

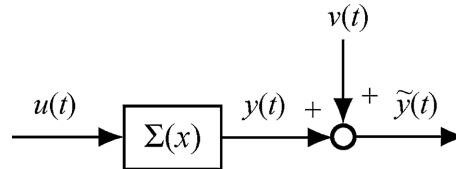


Figure 1. An identification system.

Figure 1 shows a block diagram of a system to be identified. Its state-space equation is given by

$$\Sigma(x) : \begin{cases} \dot{x}(t) = Ax(t) + Bu(t) \\ y(t) = Cx(t) + Du(t) \end{cases}, \quad (4)$$

where t is the continuous time. $u \in \mathcal{R}^m$ is the input, $y \in \mathcal{R}^p$ is the output, and $x \in \mathcal{R}^n$ is the state vector. The measurable output is given by

$$\tilde{y}(t) = y(t) + v(t). \quad (5)$$

where $v \in \mathcal{R}^p$ is the measurement noise. The input and the output for identification, denoted as ID-input and ID-output, are therefore given by

$$\text{ID-input: } u(t), \text{ ID-output: } \tilde{y}(t)$$

As a matter of fact, in the system identification calculation, discrete-time signals sampled with a constant sampling interval T_s are used. To distinguish the discrete-time signals from the continuous-time signals, the discrete-time input obtained by sampling at $t = kT_s$ is denoted as

$$u[k] \triangleq u(kT_s) \quad (k = 0, 1, 2, \dots). \quad (6)$$

Other discrete-time signals are similarly denoted. The objective of the identification in this paper is to estimate the continuous-time LTI system Equation (4) using N paired discrete-time ID-input and ID-output data

$$\{u[k], \tilde{y}[k]\} \quad (k = 0, 1, 2, \dots, N - 1). \quad (7)$$

The identification procedures are given as follows, where the order of the system n is known.

Step 1: Using N paired discrete-time ID-input and ID-output data (7), the following discrete-time LTI model is estimated using a subspace identification method.

$$\begin{cases} \xi[k+1] = P_d \xi[k] + Q_d u[k] \\ y[k] = R_d \xi[k] + S_d u[k] \end{cases}, \quad (8)$$

where $\xi \in \mathcal{R}^n$ is a state vector used in the estimated model.

Step 2: A continuous-time LTI model is obtained by inversely transforming Equation (8) with the zero-th order hold; that is,

$$\begin{cases} \dot{\xi}(t) = \mathbf{P}\xi(t) + \mathbf{Q}u(t) \\ y(t) = \mathbf{R}\xi(t) + \mathbf{S}u(t) \end{cases} \quad (9)$$

where

$$\begin{bmatrix} \mathbf{P} & \mathbf{Q} \\ \mathbf{0} & \mathbf{0} \end{bmatrix} = \frac{1}{T_s} \ln \begin{bmatrix} \mathbf{P}_d & \mathbf{Q}_d \\ \mathbf{0} & \mathbf{I}_m \end{bmatrix}, \quad \mathbf{R} = \mathbf{R}_d, \quad \mathbf{S} = \mathbf{S}_d \quad (10)$$

3.2. Identification with Actuator

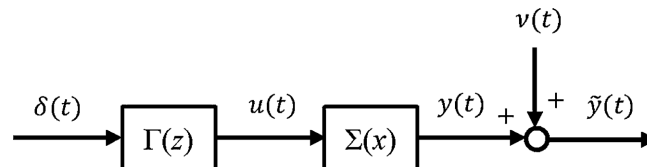


Figure 2. An identification system combined with actuator.

Figure 2 shows a system combined with an actuator system $\Gamma(z)$. It is assumed that $\Gamma(z)$ is known in advance. Its state-space equation is given by

$$\Gamma(z): \begin{cases} \dot{z}(t) = \mathbf{F}z(t) + \mathbf{G}\delta(t) \\ \mathbf{u}(t) = \mathbf{H}z(t) \end{cases}, \quad (11)$$

where $\delta \in \mathcal{R}^m$ is the command input to the actuator system, and $z \in \mathcal{R}^{2m}$ is state vector. In this paper, the actuator is given by the second-order model for each input channel. The state-space equation of the i -th actuator is given by

$$\begin{cases} \dot{z}_i(t) = \mathbf{F}_i z_i(t) + \mathbf{G}_i \delta_i(t) \\ \mathbf{u}_i(t) = \mathbf{H}_i z_i(t) \end{cases} \quad (i = 1, \dots, m), \quad (12)$$

where $z_i \in \mathcal{R}^2$ and

$$\mathbf{F}_i = \begin{bmatrix} 0 & 1 \\ -\omega_i^2 & -2\zeta_i\omega_i \end{bmatrix}, \quad \mathbf{G}_i = \begin{bmatrix} 0 \\ \omega_i^2 \end{bmatrix}, \quad \mathbf{H}_i = [1 \quad 0] \quad (i = 1, \dots, m). \quad (13)$$

The matrices and the vectors of Equation (11) are then constructed as

$$\begin{aligned} \mathbf{F} &\triangleq \text{block} \cdot \text{diag} \{ \mathbf{F}_1 \cdots \mathbf{F}_m \}, & \mathbf{G} &\triangleq \text{block} \cdot \text{diag} \{ \mathbf{G}_1 \cdots \mathbf{G}_m \}, \\ \mathbf{H} &\triangleq \text{block} \cdot \text{diag} \{ \mathbf{H}_1 \cdots \mathbf{H}_m \}. \end{aligned} \quad (14)$$

$$\boldsymbol{\delta} \triangleq [\delta_1 \cdots \delta_m]^\top, \quad \mathbf{u} \triangleq [u_1 \cdots u_m]^\top, \quad \mathbf{z} \triangleq [z_1 \cdots z_m]^\top. \quad (15)$$

Table 1 shows the choices of ID-input and ID-output for the system identification with actuator. id-0 indicates the case without actuator system, while the rest are the cases with the actuator system. id-1 is the case in which ID-input is given by $\delta(t)$. id-2 is the case in which ID-input is given by $\mathbf{u}(t)$ which is the output from the actuator system. A measurement is needed to obtain $\mathbf{u}(t)$. id-3 is the case that the measurement noise $\mathbf{w}(t)$ is taken into consideration in ID-input; that is,

$$\tilde{\mathbf{u}}(t) = \mathbf{u}(t) + \mathbf{w}(t). \quad (16)$$

Table 1. Input and output for identification.

	ID-input	ID-output	Status
id-0	$u(t)$	$\tilde{y}(t)$	Figure 1
id-1	$\delta(t)$	$\tilde{y}(t)$	Figure 2
id-2	$u(t)$	$\tilde{y}(t)$	Figure 2
id-3	$\tilde{u}(t)$	$\tilde{y}(t)$	Figure 2

4. Setup for Identification

4.1. Maximal Length Sequence

Maximal length sequence (M-sequence) [13]-[15] is a binary signal having values of $\{0, 1\}$ or $\{-1, 1\}$. The persistent excitation condition holds [1]; that is, the M-sequence can be used as an exciting signal. In general, the effective frequency range of the discrete-time signal with the sampling interval T_s is given by $[0, \omega_N]$, where ω_N is the Nyquist frequency defined as $\omega_N = \pi/T_s$. However, it may be impossible to realize fast excitation because of the frequency characteristic limits of the actuators for control surfaces of aircraft. In this paper, the required activities of the control surfaces are specified by the bandwidth ratio of the M-sequence, denoted as B_M . Letting T_i be the minimum time length where the value of the M-sequence is not changed, B_M is defined as

$$B_M \triangleq \frac{T_s}{T_i}. \quad (17)$$

4.2. Identification Index

This subsection presents the identification indexes. The two indexes are related to the dynamical modes of aircraft [11]. In the following, the subscript # corresponds to the longitudinal dynamical modes of aircraft: sp : short-period and lp : long-period modes. The first is the bandwidth ratio for the dynamical mode, which is defined as

$$B_{\#} \triangleq \frac{\omega_N B_M}{\omega_{\#}}. \quad (18)$$

$B_{\#} > 1$ indicates that the bandwidth of the M-sequence is covered beyond that of the dynamical mode. Since $\omega_{sp} > \omega_{lp}$ in the longitudinal motion, we have $B_{sp} < B_{lp}$. Then, if B_{sp} is greater than one, the M-sequence is able to excite both the short- and long-period modes.

The other is the ratio of data for the dynamical mode which is defined as

$$R_{\#} \triangleq \frac{\omega_{\#} N}{2\omega_N}. \quad (19)$$

$R_{\#} > 1$ indicates that the amount of data for identification is greater than the period of the dynamical mode. In longitudinal motion, we have $R_{sp} > R_{lp}$. Then,

if R_{lp} is greater than one, the number of data used for identification is greater than that of data needed for the period of the longitudinal dynamical modes.

When actuators for control surfaces are considered, another index is the bandwidth ratio between the actuator and the dynamical mode. It is defined as

$$W_{\#} \triangleq \frac{\omega_a}{\omega_{\#}}. \quad (20)$$

where ω_a is the natural frequency of the actuator. When multiple actuator models are needed as Equations (11)-(15), ω_a is given by

$$\omega_a \triangleq \min\{\omega_i\} \quad (i = 1, \dots, m). \quad (21)$$

$W_{\#} > 1$ indicates that the bandwidth of the actuators is able to excite the dynamical modes of aircraft. Since $\omega_{sp} > \omega_{lp}$ in the longitudinal motion, we have $W_{sp} < W_{lp}$. Then, W_{sp} is used as an index to characterize the actuator in this paper.

4.3. Evaluation of Identification

Identification results are generally evaluated from several standpoints: visual and numerical methods, global and local viewpoints. The time and frequency responses are visual and global evaluations. As a numerical evaluation, this paper adopts the ν -gap metric and the additive pole error of the dynamical modes. These definitions are given as follows.

4.3.1. ν -Gap Metric

Let the transfer functions of the true and estimated continuous-time linear models be $P^*(s)$ and $\hat{P}(s)$, respectively, where s is the Laplace operator. The ν -gap metric, denoted as δ_{ν} , is defined as

$$\delta_{\nu} \triangleq \sup_{\omega} \kappa\left(\hat{P}(j\omega), P^*(j\omega)\right). \quad (22)$$

where

$$\kappa(X, Y) \triangleq \bar{\sigma}\left[\left(I + Y\bar{Y}\right)^{-1/2} (Y - X)\left(I + X\bar{X}\right)^{-1/2}\right].$$

$\bar{X}(s)$ is the conjugate transfer function of $X(s)$ and $\bar{\sigma}[\cdot]$ is the maximum singular value. The range of δ_{ν} is normalized as $\delta_{\nu} \in [0, 1]$ [16]. δ_{ν} represents a measure of the difference between two LTI systems in the frequency response. Therefore, δ_{ν} is one of the global evaluations. δ_{ν} is originally derived from the robust stability condition based on the normalized coprime factorization [16]. It is desirable in system identification that δ_{ν} should be as small as possible.

4.3.2. Pole Error of Dynamical Mode

Letting the true and estimated eigenvalues of the dynamical mode $\lambda_{\#}$ be $\lambda_{\#}^*$ and $\hat{\lambda}_{\#}$, respectively, the additive pole error of dynamical mode is defined as

$$\varepsilon_a(\lambda_{\#}) \triangleq \left| \hat{\lambda}_{\#} - \lambda_{\#}^* \right|. \quad (23)$$

This is a local evaluation of the identified model.

5. Numerical Simulation

This section presents numerical simulation results of longitudinal aircraft model identification according to the setup for identification described in the previous section. The aircraft to be identified is referenced from Isozaki *et al.* [17]. The flight conditions were given for the following steady straight flight: altitude $H = 4000$ [m], flight velocity $U = 100$ [m/s], and steady pitch angle $\Theta = 0$ [deg]. The eigenvalues of the dynamical modes were $\lambda_{sp}, \bar{\lambda}_{sp} = -0.9994 \pm j2.0052$ and $\lambda_{lp}, \bar{\lambda}_{lp} = -0.0076 \pm j0.1366$.

The subspace identification method used was N4SID [3] [4]. The sampling interval was given as $T_s = 0.1$ [s]. The M-sequence was used for exciting the actuators of the control surfaces of the aircraft, where the amplitudes of the commands were given as $\delta_e, \delta_t = \pm 3$ [deg]. The measurement noises $\mathbf{v}(t)$ and $\mathbf{w}(t)$ were given as the white noises whose magnitude was defined by the noise-signal ratio (NSR)

$$NSR_v \triangleq \left(\frac{\frac{1}{N} \sum_{k=1}^N \|\mathbf{v}[k]\|_2^2}{\frac{1}{N} \sum_{k=1}^N \|\mathbf{y}[k]\|_2^2} \right) \times 100(\%), \quad NSR_w \triangleq \left(\frac{\frac{1}{N} \sum_{k=1}^N \|\mathbf{w}[k]\|_2^2}{\frac{1}{N} \sum_{k=1}^N \|\mathbf{u}[k]\|_2^2} \right) \times 100(\%) \quad (24)$$

That is, NSR_v and NSR_w indicate the mean amplitude ratios between the measurement noises and the true output and input, respectively. Generally speaking, the identification performance deteriorates as the NSR_v increases. The identification results were evaluated by averaging 10 times trials where the NSR_v was given as $NSR_v = \{10, 20, \dots, 100\}$ (%).

5.1. Identification Results of $W_{sp} = 2$ and 6

The identification results with considering actuator are shown in Table 2 and Figures 3-5. The magnitude of the measurement noises $\mathbf{v}(t)$ and $\mathbf{w}(t)$ were given by $NSR_v = 30\%$ and $NSR_w = 20\%$, respectively. “true” in the figures means the responses and the location of the true longitudinal aircraft model.

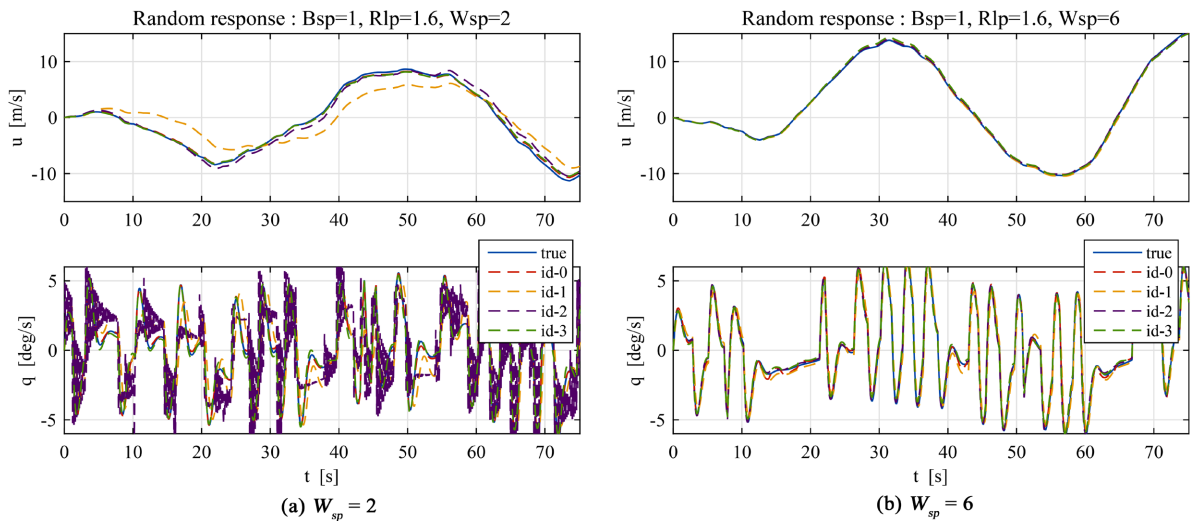


Figure 3. Random responses of flight velocity u and pitch rate q in the identified longitudinal model.

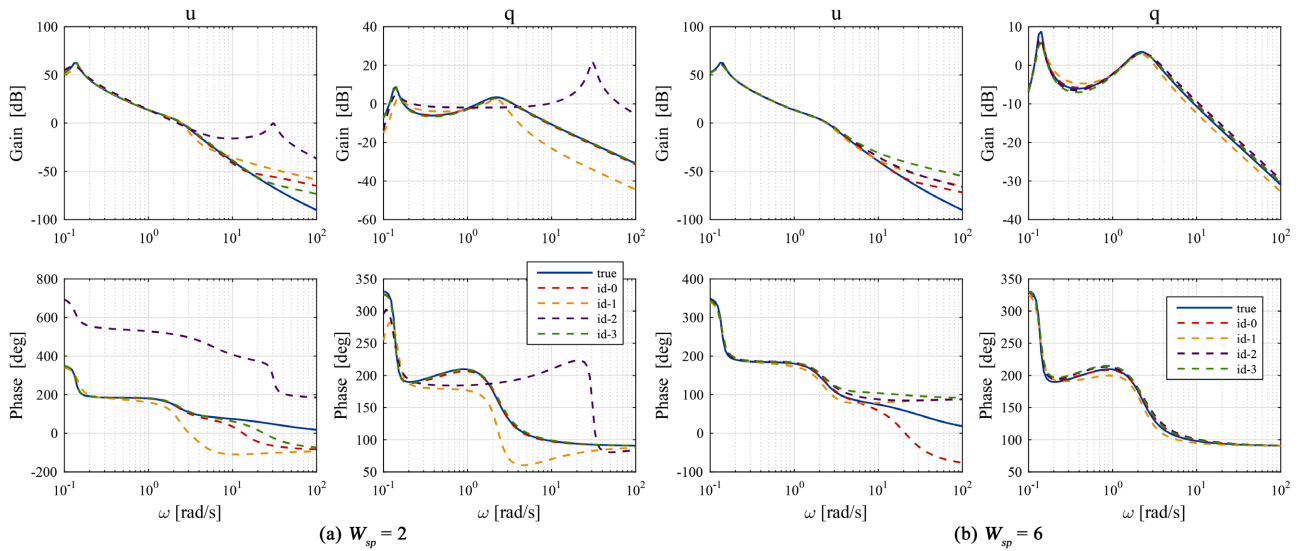


Figure 4. Frequency responses of flight velocity u and pitch rate q in identified longitudinal model.

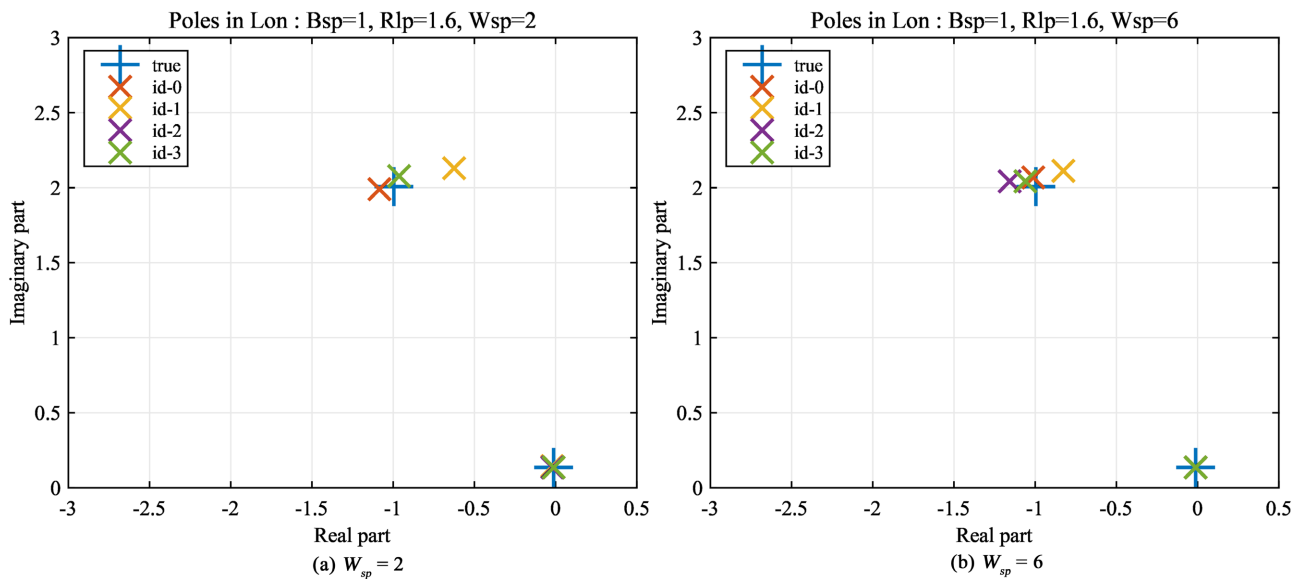


Figure 5. Pole location of the identified longitudinal model.

In the cases of $W_{sp} = 2$ in Table 2 and Figure 5, compared with id-0, which is the case without an actuator, the identification performance of id-1 and id-2 has deteriorated; in particular, $\varepsilon_a(\lambda_{sp})$ of id-1 and id-2 was greater than that of id-0. The influence of $\varepsilon_a(\lambda_{sp})$ appeared in δ , the random and frequency responses. In particular, the pitch rate q in id-2 showed vibrational responses, which were close to unstable responses, as shown in Figure 3(a). The peak gain of q in id-2 was shifted to the higher frequency region, as shown in Figure 4(a).

In the cases of $W_{sp} = 6$, on the other hand, the identification performance of id-1 and id-2 was close to that of id-0. The performance of id-3 was almost the same level as that of id-0 in both $W_{sp} = 2$ and 6. The details will be discussed later. The condition number [18], denoted as “Cond” shown in Table 2, will also

be mentioned. It is seen from **Figure 5** that λ_{lp} of id-1 and id-2 almost coincided with the true location. This means that the long-period mode was not influenced by the actuator.

Table 2. Identification results of longitudinal model, where $B_{sp} = 1.0$, $R_{lp} = 1.6$, $W_{sp} = 2$ and 6.

	W_{sp}	δ_v	$\varepsilon_a(\lambda_{sp})$	$\varepsilon_a(\lambda_{lp})$	Cond
id-0	2	0.0396	0.0878	0.00210	1.1707×10^3
id-1	2	0.5149	0.3935	0.01555	7.2338×10^2
id-2	2	0.9883	29.4131	0.00976	4.0727×10^4
id-3	2	0.0465	0.0763	0.00317	1.6353×10^3
id-0	6	0.0636	0.0647	0.00153	1.6759×10^3
id-1	6	0.1473	0.2024	0.00145	1.3880×10^3
id-2	6	0.0774	0.1601	0.00100	2.2071×10^3
id-3	6	0.0485	0.0700	0.00177	1.8004×10^3

5.2. Influence of B_{sp} and W_{sp}

In the aircraft model identification without an actuator [11], B_{sp} was strongly related to $\varepsilon_a(\lambda_{sp})$, while R_{lp} was to $\varepsilon_a(\lambda_{lp})$. The reversed pairs were not related so much. Therefore, this subsection discusses the identification performance of id-1 and id-2 with respect to B_{sp} and W_{sp} , where R_{lp} was fixed at $R_{lp} = 1.6$.

Figure 6 shows δ_v and $\varepsilon_a(\lambda_{sp})$ with respect to W_{sp} . When W_{sp} was increased, δ_v and $\varepsilon_a(\lambda_{sp})$ were monotonously decreased. Furthermore, the identification performance of id-1 and id-2 was improved by increasing B_{sp} . The performance

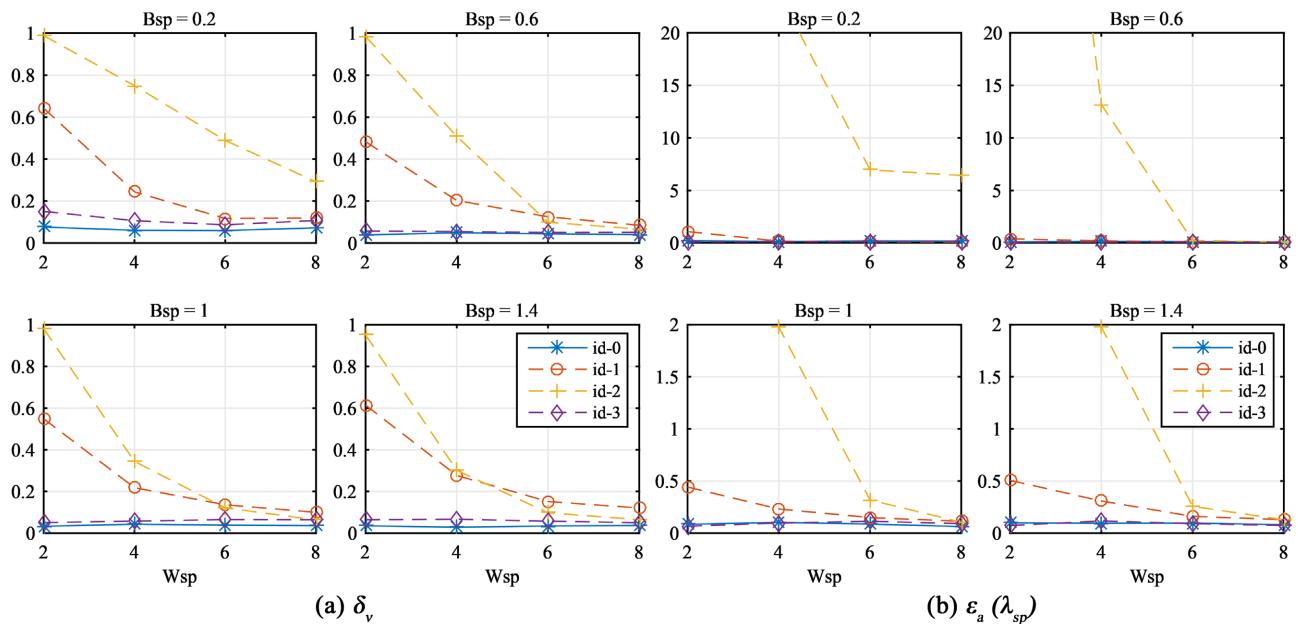


Figure 6. Identification evaluation with respect to B_{sp} and W_{sp} .

was converged to that of id-0 when $B_{sp} \geq 1.4$ and $W_{sp} = 8$. This is the lower limit of the identification with the actuator. In the region of small B_{sp} and W_{sp} , δ_v of id-1 was better than that of id-2. In the region of large B_{sp} and W_{sp} , on the other hand, this situation was changed as shown in **Figure 6(a)**.

5.3. Influence of Measurement Noise $w(t)$

Figure 7 shows the identification result with respect to the input noise $w(t)$; that is, the case of id-3. When B_{sp} and W_{sp} were small, there was the minimum region of δ_v and $\varepsilon_a(\lambda_{sp})$ around $NSR_w = 20\%$. According to the increase of B_{sp} and W_{sp} , the minimum region became ambiguous. It disappeared for $B_{sp} \geq 0.6$ and $W_{sp} = 8$. NSR_w of id-3 shown in **Figure 6** was given by $NSR_w = 20\%$. The identification performance of id-3 was almost the same as that of id-0 for the range of $W_{sp} \in [2, 8]$.

As mentioned above, $\tilde{u}(t)$ was contributed to improving the performance of aircraft model identification with actuators. The time history of ID-input, the elevator angle δ_e and the throttle angle δ_t for $B_{sp} = 1.0$ and $W_{sp} = 2$ was shown in **Figure 8**, where $\delta(t)$, $u(t)$ and $\tilde{u}(t)$ are ID-input of id-1, id-2 and id-3, respectively. The NSR of $w(t)$ included in $\tilde{u}(t)$ was given by $NSR_w = 20\%$. The response of $u(t)$ was delayed due to the dynamics of the actuators. Furthermore, to investigate this from the frequency characteristic point of view, **Figure 9** shows the spectra of δ_e in $\delta(t)$, $u(t)$ and $\tilde{u}(t)$. Two magenta asterisks indicate the natural frequencies of the short- and the long-period modes. The spectra of the three input signals were large in the frequency region shown by red triangle-line. This means that the bandwidth of ID input covers the range of dynamical modes. In the high-frequency region, the spectrum in $\delta(t)$ was decreased, but a specific magnitude was kept until the Nyquist frequency $\omega_N = 31.4$ [rad/s]. On the other hand, the spectrum in $u(t)$ was further reduced, while that in $\tilde{u}(t)$ was recovered by the noise $w(t)$.

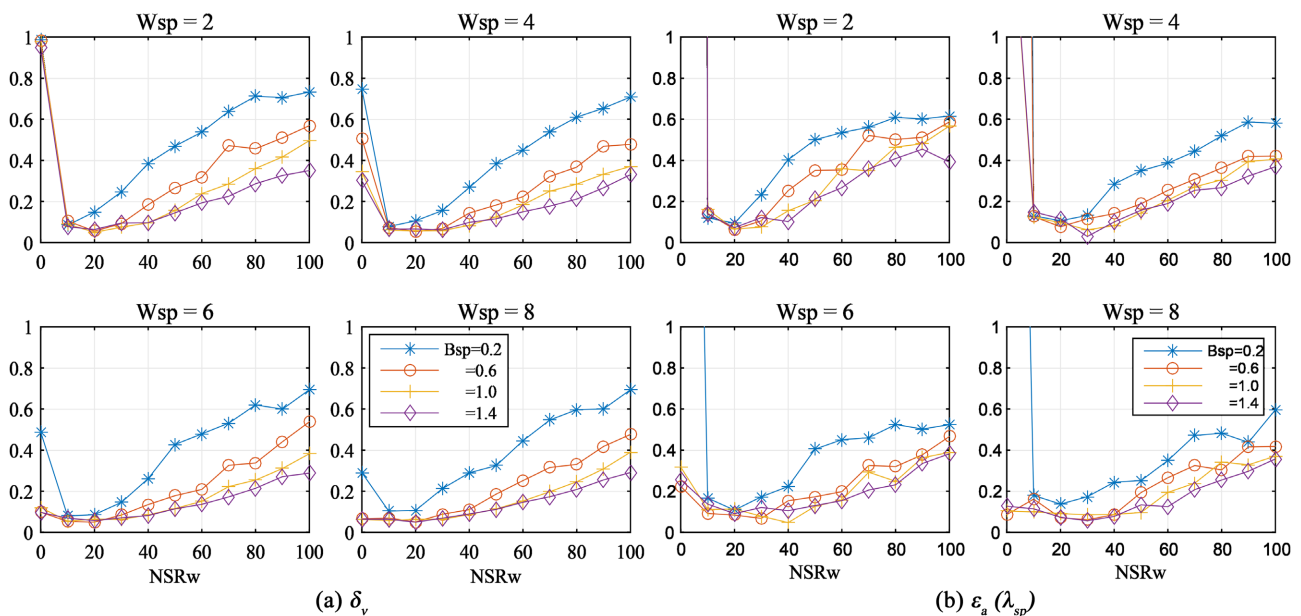


Figure 7. Identification evaluation with respect to NSR_w .

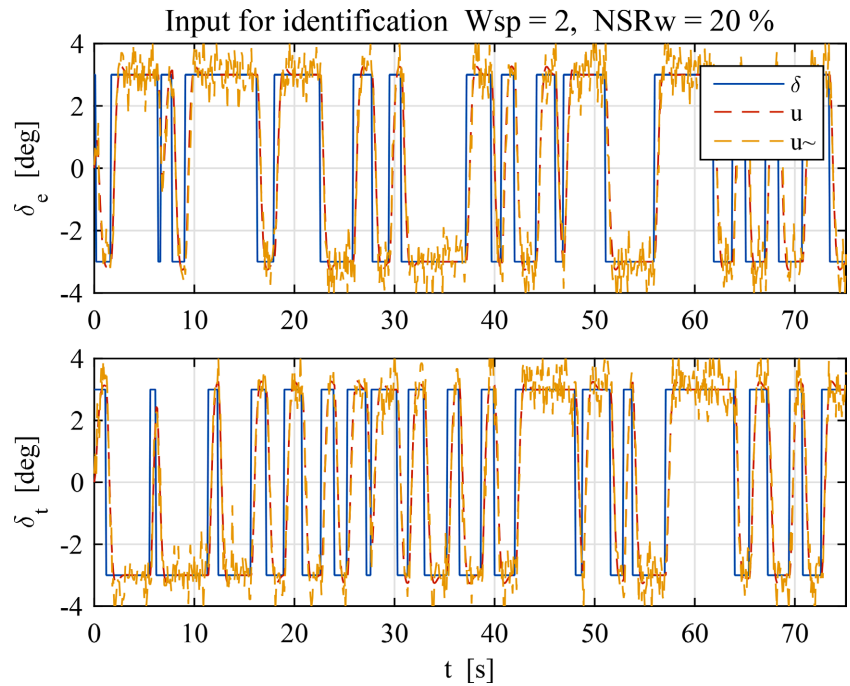


Figure 8. ID-inputs for longitudinal model, where δ_e and δ_t are elevator and throttle angles.

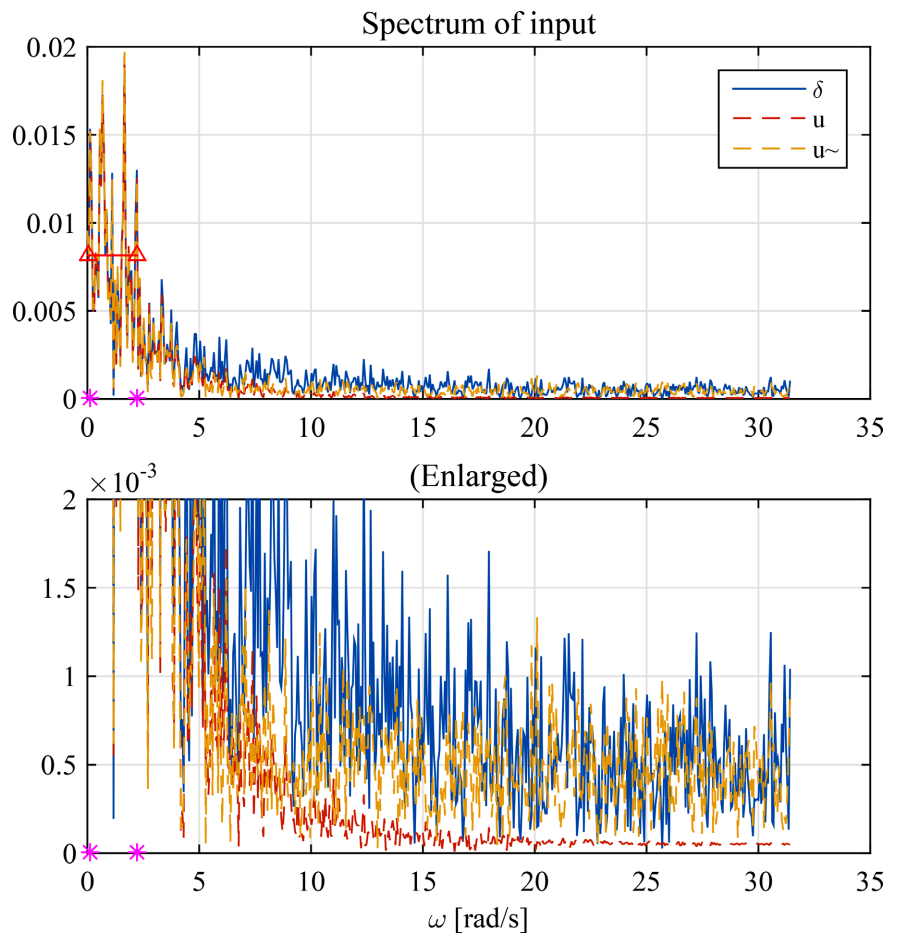


Figure 9. Spectrum of δ_e included in $\delta(t)$, $u(t)$ and $\tilde{u}(t)$.

It may be possible to explain the effectiveness of the spectrum recovery in the identification performance as follows. In the N4SID method, the matrices of the estimated discrete-time model in **Step 1** shown in Section 2.1 are obtained by applying the least square method to the following linear equation

$$\begin{bmatrix} X_{k+1} \\ Y_k \end{bmatrix} = \begin{bmatrix} P_d & Q_d \\ R_d & S_d \end{bmatrix} \begin{bmatrix} X_k \\ U_k \end{bmatrix} \quad (25)$$

where $U_k \in \mathcal{R}^{m \times N}$ and $Y_k \in \mathcal{R}^{p \times N}$ are respectively constructed by ID-input and ID-output, and $X_k \in \mathcal{R}^{n \times N}$ is obtained by LQ- and SV-decomposition [3] [4]. It is, in general, known in numerical computation that the accuracy of the solution depends on the algorithm and the condition of the problem [19]. Since the N4SID method was used for all identification calculations, the accuracy of the solution depended on the latter. The right-hand side column in **Table 2**, denoted as “Cond”, shows the condition number of $\Phi_k \Phi_k^T$, where $\Phi_k \triangleq \begin{bmatrix} X_k^T & U_k^T \end{bmatrix}^T$. In general, a large condition number means *ill-conditioned*; that is, easily brings a large error in the solution, while a small condition number means *well-conditioned* [18] [19]. As shown in **Table 2**, the Cond of id-2 in $W_{sp} = 2$ was larger than that of the others, while it became small in $W_{sp} = 6$. As a matter of fact, the identification performance of id-2 in $W_{sp} = 6$ was improved. Since the input noise $w(t)$ was included in U_k it contributed to the reduction of the condition number. This was a reason from the numerical computational point of view why the identification performance of id-3 was superior to that of id-1 and id-2.

6. Concluding Remarks

This paper has presented an identification of a continuous-time linear aircraft model considering control surface actuators using the maximal length sequence (M-sequence) signal. In the identification with the actuator, the input for identification was given by the command to the actuator or the output from the actuator. The identification results using these inputs were evaluated by the v-gap metric and the pole error of the dynamical modes. In the numerical simulation of longitudinal aircraft model identification, the identification performance was improved when the bandwidth ratio for the short-period mode and the bandwidth ratio between the actuator and the short-period mode were increased. Furthermore, a little input noise brought an improvement in the identification performance. This may be effective in the case that the bandwidth ratio for the short-period mode and/or the actuator and the short-period mode are not sufficiently large in practical system identification. The results presented in this paper are, therefore, also useful to other system identification problems. Although this paper presented a numerical simulation of longitudinal aircraft model identification, similar results had been obtained in the simulation of lateral aircraft model identification.

Conflicts of Interest

The authors declare no conflicts of interest regarding the publication of this paper.

References

- [1] Ljung, L. (1999) System Identification—Theory for the User. 2nd Edition, Prentice Hall.
- [2] Soderstrom, T. and Stoica, P. (1989) System Identification. Prentice Hall.
- [3] Verhaegen, M. and Verdult, V. (2007) Filtering and System Identification. Cambridge University Press. <https://doi.org/10.1017/cbo9780511618888>
- [4] Overschee, P. and Moor, B. (1996) Subspace Identification for Linear Systems: A Least Squares Approach. Kluwer Academic Publishers.
- [5] Yadav, D.K., Kulkarni, A. and Yao, H. (2022) A Comparative Study of Managing a Project Using Traditional Management Techniques and a Critical Chain Project Management Methodology in Aircraft Maintenance Field. *Journal of Transportation Technologies*, **12**, 544-558. <https://doi.org/10.4236/jtts.2022.124032>
- [6] Karimanzira, D. and Rauschenbach, T. (2020) Deep Learning Based Model Predictive Control for a Reverse Osmosis Desalination Plant. *Journal of Applied Mathematics and Physics*, **8**, 2713-2731. <https://doi.org/10.4236/jamp.2020.812201>
- [7] Sekerere, K., Ndeda, R. and Kabini, K. (2023) An Investigation of the Effects of Thermal Interference between Adjacent Nitinol Spring Actuators in a Tactile Display. *World Journal of Engineering and Technology*, **11**, 136-152. <https://doi.org/10.4236/wjet.2023.111010>
- [8] Schmidt, L.V. (1998) Introduction to Aircraft Flight Dynamics. American Institute of Aeronautics and Astronautics. <https://doi.org/10.2514/4.862052>
- [9] Fujimori, A. (2016) Identification of Continuous-Time Linear Aircraft Models Using Subspace Identification. *Journal of Aerospace Science and Technology*, **2**, 7-12. <https://doi.org/10.17265/2332-8258/2016.01.002>
- [10] Sakashita, K. (2016) Continuous-Time Linear Modeling for Aircraft Using Subspace Identification, Graduation Thesis, University of Yamanashi.
- [11] Fujimori, A. and Oh-Hara, S. (2021) An Effective Maximal-Length Sequence Design for System Identification of a Continuous-Time Linear Aircraft Model. *Transactions of the Japan Society for Aeronautical and Space Sciences*, **64**, 215-222. <https://doi.org/10.2322/tjsass.64.215>
- [12] Mochizuki, K. (2023) System Identification of Aircraft Models Using Subspace Identification, Master Thesis, University of Yamanashi.
- [13] Golomb, S.W. and Gong, G. (2005) Signal Design for Good Correlation: For Wireless Communication, Cryptography, and Radar. Cambridge University Press. <https://doi.org/10.1017/cbo9780511546907>
- [14] Buračas, G.T. and Boynton, G.M. (2002) Efficient Design of Event-Related fMRI Experiments Using M-Sequences. *NeuroImage*, **16**, 801-813. <https://doi.org/10.1006/nimg.2002.1116>
- [15] Poudel, K.N. and Robertson, W.M. (2018) Maximum Length Sequence Dielectric Multilayer Reflector. *OSA Continuum*, **1**, 358. <https://doi.org/10.1364/osac.1.000358>
- [16] Vinnicombe, G. (2000) Uncertainty and Feedback—H_∞ Loop-Shaping and the N-Gap Metric. Imperial College Press. <https://doi.org/10.1142/9781848160453>
- [17] Isozaki, K., Masuda, K., Taniuchi, A., and Watari, M. (1980) Flight Test Evaluation of Variable Stability Airplane, KHI. *Technology Reviews*, **75**, 50-58.
- [18] van der Sluis, A. (1969) Condition Numbers and Equilibration of Matrices. *Numerische Mathematik*, **14**, 14-23. <https://doi.org/10.1007/bf02165096>
- [19] Forsythe, G.E., Malcolm, M.A. and Moler, C.B. (1977) Computer Methods for Mathematical Computations. Prentice-Hall.